Brazilian Journal of Physics
ISSN: 0103-9733
luizno.bjp@gmail.com
Sociedade Brasileira de Física
Brasil

Hernández-García, Anier; Fernández Barbero, Antonio; Sotolongo-Costa, Oscar
Non-Steady Wall-Bounded Flows of Viscoelastic Fluids Under Periodic Forcing
Brazilian Journal of Physics, vol. 44, núm. 4, 2014, pp. 315-325
Sociedade Brasileira de Física
Sâo Paulo, Brasil

Braz J Phys (2014) 44:315–325
DOI 10.1007/s13538-014-0211-0

SOCIEDADE BRASILEIRA DE FÍSICA

CONDENSED MATTER

Non-Steady Wall-Bounded Flows of Viscoelastic Fluids Under Periodic Forcing

Anier Hernández-García · Antonio Fernández Barbero · Oscar Sotolongo-Costa

Received: 15 February 2013 / Published online: 12 June 2014

Abstract The problem of oscillating flows inside pipes under periodic forcing of viscoelastic fluids is addressed here. Starting from the linear Oldroyd-B model, a generalized Darcy's law is obtained in the frequency domain and an explicit expression for the dependence of the dynamic permeability on the fluid parameters and forcing frequency is derived. Previous results in both viscoelastic and Newtonian fluids are here shown to be particular cases of our results. On the basis of our calculations, a possible explanation for the observed damping of local dynamic response as the forcing frequency increases is given. Good fitting with recent experimental studies of wave propagation in viscoelastic media is here exhibited. Sound wave propagation in viscoelastic media flowing inside straight pipes is investigated. In particular, we obtain the local dynamic response for weakly compressible flows.

Keywords Dynamics of oscillating viscoelastic solutions · Oldroyd-B model · Sound wave propagation in viscoelastic media

A. Hernández-García
Niels Bohr Institute, University of Copenhagen,
Blegdamsvej 17, DK-2100 Copenhagen, Denmark

A. Hernández-García (✉) · O. Sotolongo-Costa
"Henri Poincaré" Group of Complex Systems,
University of Havana, Havana, Cuba
e-mail: ahernan@nbi.ku.dk

O. Sotolongo-Costa
Physics Department, Faculty of Sciences, Morelos Autonomous University, Morelos, Mexico

A. Fernández Barbero
Group of Complex Fluids, Almeria University, Almeria, Spain

1 Introduction

Wall-bounded oscillating flows of Newtonian fluids driven by periodic forcing have been extensively studied both theoretically and experimentally. Interesting phenomena such us the formation of non-steady boundary layers have been observed, provided that the frequency of the applied force is larger than the inverse of the characteristic time in which the vorticity diffuses along the cross-section (see for instance [1] and references therein). Recently, the formation of a non-steady boundary layer has also been predicted for Oldroyd-B fluids [2].

In recent advances in many topics ranging from soft-matter, biofluid mechanics, rocket propulsion, rheology among others are encountered flows in which Newtonian approximation breaks down. Remarkably, it has been recently observed in oscillating wall-bounded flows of these fluids that when relaxation times of elastic stresses are comparable with characteristics times scales of the flow, the nontrivial interactions of elastic degrees of freedom with the inertial ones and flow geometry give rise to a resonant like behavior that is absent in the corresponding Newtonian flow [4, 5, 7]. More recently, it has been observed that these basic oscillating parallel shear flows become unstable as the frequency and/or the amplitude of oscillations are increased [6]. In contrast to the observed instabilities in Newtonian fluids, these instabilities take place at vanishingly small Reynolds numbers. As a consequence, inertial effects are negligible and these instabilities are of a pure elastic nature caused by anisotropies in the viscoelastic stress tensor induced by the large shear flow rates formed in the oscillating flows. As this instability develops, many properties of the flow such mass and heat transport might change dramatically throughout the entire system as the flow become rather chaotic. Thus, the description of

oscillating wall-bounded flows of non-Newtonian fluids is of great importance for both fundamental physics and applied topics.

In [5, 7], by means of velocity measurements at the center of a viscoelastic fluid column ($NayCl/NaSal$ *in water*) flowing inside a straight pipe of circular cross section [5] and more recently in the entire cross section of the fluid column [7], it was found a dramatic enhancement in the dynamic response to an oscillating periodic pressure gradient, that is, the fluid response, measured in terms of the velocity for a given amplitude of the pressure gradient, exceeds by several orders in magnitude that obtained for the steady case. It is noteworthy that most of the features observed in experiments, namely the values of the driving frequencies at which the resonant behavior takes place and the formation of Couette-like flows as the driving frequency increases, are successfully reproduced by a linear Navier-Stokes and Maxwell constitutive equations [4, 7, 8]. Nevertheless, theoretical predictions within this model overestimate the magnitude of the response amplitude as well as the root mean square velocity at the pipe axis and the velocity at certain points of the cross section of the fluid column. Furthermore, the Maxwell model cannot describe the damping observed in the peaks of dynamic permeability as the driving frequency is increased (at least in the range of frequencies covered by both experiments). These issues motivated us to extend earlier theoretical works in the hope that this may shed light on the the physical mechanisms that could lead to the observed phenomena.

In this article, specifically, we shall try to assess the effects that pure Newtonian contributions (due to the solvent) to the total stress tensor of viscoelastic solutions will have on the fluid response in wall-bounded oscillating flows under periodic forcing. In order to achieve that, we shall assume that stresses in the viscoelastic solution obey the linear Oldroyd-B constitutive equation [9–11]. In particular, we present a detailed theoretical derivation of the velocity field and the dynamic permeability in flows at small both Reynolds and Weissenberg numbers. As we shall see, our findings suggest that the (additional) Newtonian component of stresses due to solvent viscosity might lead to the damping of the local dynamic response as the forcing frequency increases, a fact observed in [5, 7]. Since, as observed in [6], some of the resonance frequencies the shear rates are sufficiently large, we qualitatively analyze the effects of nonlinearities of the full Oldroyd-B constitutive equation on parallel oscillating shear flows by means of a perturbation scheme. This scheme led us to find a criterion for the onset of the elastic instability which, as stated below, agrees with the findings reported in [6]. We also investigate the behavior of the local dynamic response and velocity profiles in weakly compressible flows. Our main purpose is to compare our findings against known results for incompressible fluids.

The article is organized as follows. In Section 2, for completeness, we briefly review main aspects of the Oldroyd-B model. In Section 3, we introduce the main assumptions and the resulting set of governing equations we have used to derive explicit expressions for the dynamic permeability, the velocity field, and the local dynamic response which are defined within this section. Here, we also compare our results with the measured values of the local dynamic response and the root mean square velocity reported in [5]. In Section 4, the problem of modeling stresses for weakly compressible flows is revisited and starting from it, a explicit expression for the local dynamic response is obtained. A comparison of the latter magnitude against the corresponding incompressible case, bearing in mind the experimental conditions, is also made.

Some of the definitions and expressions presented in this article have already been presented in previous publications. Wherever needed, we shall repeat them for the sake of clarity and completeness.

2 Oldroyd-B Model

One of the simplest models that describes basic viscoelastic behavior of an incompressible liquid having a constant shear viscosity, and constant relaxation and retardation times, is the so-called Oldroyd-B model [9–11]. This is an extension of the Maxwell model that fits quite well data from polymeric solutions.

In the Oldroyd-B model, it is considered that viscoelastic fluids can be regarded as a dilute suspension of elastic dumbbells. Thus, the complicated structure of the molecules that form the liquid is replaced by a simpler mechanical structure consisting of identical pairs of microscopic beads (of negligible mass) connected by Hookean springs. Besides, the concentration is supposed to be uniform and very low. The latter ensures that polymer-polymer interactions are negligible. Furthermore, the viscoelastic solution is regarded as a continuous medium. The "coarsening" involved in such description requires to get rid of the microscopic degrees of freedom. Consequently, the reaction of the dumbbells on the fluid is treated at a mean field level described by an elastic contribution σ^e to the total stress tensor, which is found to be proportional to the conformation tensor , i.e.,

$$\sigma^e_{ij} \propto < R_i R_j >, \tag{1}$$

where R_i denotes the ith component of the elongation vector (obtained by subtracting the position of one bead from that of the other one). In Eq. (1), the average is taken over the statistics of the thermal noise, or equivalently over a volume

large enough to contain a huge number of molecules but small compared with the whole fluid volume. The conformation tensor is defined as $\sigma_{ij}^c = \frac{<R_i R_j>}{R_0^2}$, where R_0 is the equilibrium length of the spring. The evolution equation for the conformation tensor can be inferred by considering the forces which act on the beads, namely, the hydrodynamic drag, which obeys a Stokes' law, a Brownian force and the elastic spring force. When details of the kinetic theory are worked out, one gets the following model incorporating the elastic nature of the dumbbells stress tensor [11–13], the so-called Maxwell model

$$\sigma^e + \lambda \frac{\delta \sigma^e}{\delta t} = \eta_p \left[\nabla v + (\nabla v)^t\right], \tag{2}$$

where η_p is the contribution of the elastic additives to the total shear viscosity in steady flows at small shear rates, $(\nabla v)_{ij} = \frac{\partial v_i}{\partial x_j}$ is the velocity gradient tensor, $(\nabla v)^t$ is its transpose, and λ is the relaxation time of elastic stresses. The symbol $\frac{\delta}{\delta t}$ denotes the upper-convected time derivative defined by [11, 14]

$$\frac{\delta G}{\delta t} = \frac{\partial G}{\partial t} + (v \cdot \nabla) G - \left[G \cdot \nabla v + (\nabla v)^t \cdot G\right] \tag{3}$$

Thus, the above time derivative takes into account that the relation between stresses and kinematic tensors at a fluid particle are independent of the instantaneous orientation of that particle. One can see that the ratio between the terms inside brackets on the right-hand side of Eq. (3) to the linear relaxation term is determined by the dimensionless expression $\lambda \frac{V}{L}$, called the Weissenberg number, where V and L are a typical velocity and length scale of the flow, respectively. For instance, in a flow inside a straight pipe, those magnitudes could be taken as the maximum value of the velocity across the cross section and the radius, respectively. We may also note that the ratio between the advection term $(v \cdot \nabla) G$ and the relaxation one is given by the Weissenberg number as well. Thus, when the latter number is sufficiently small, the relaxation of elastic stresses overcomes the effects caused by nonlinearities in the constitutive equations (2) and (3). In this limit, the upper-convected derivative could be replaced by the local time derivative

$$\frac{\delta G}{\delta t} \simeq \frac{\partial}{\partial t}. \tag{4}$$

In the Oldroyd-B model, the total stress tensor σ is given by the sum of a Newtonian solvent contribution σ^s and the elastic additives contribution σ^e, i.e.,

$$\sigma = \sigma^e + \sigma^s. \tag{5}$$

The constitutive equation for the solvent is given by

$$\sigma^s = \eta_s \left[\nabla v + (\nabla v)^t\right], \tag{6}$$

where η_s is the solvent viscosity.

When the two contributions are added, the result is found to be

$$\sigma + \lambda \frac{\delta \sigma}{\delta t} = \eta_0 \left(\mathbf{D} + \lambda \frac{\eta_s}{\eta_0} \frac{\delta \mathbf{D}}{\delta t}\right), \tag{7}$$

where $\mathbf{D} = \nabla v + (\nabla v)^t$ is the symmetric part of the velocity gradient tensor, and $\eta_0 = \eta_s + \eta_p$.

From the above expression, the Maxwell's model is recovered making $\eta_s \to 0$. Moreover, if we let $\lambda \to 0$, the Newtonian model is obtained.

3 Non-Steady Flow of Oldroyd-B Liquids in Straight Cylindrical Pipes

3.1 Set of Governing Equations

We shall now proceed to derive an analytical expression of the velocity field of an Oldroyd-B liquid subject to an oscillatory pressure gradient and confined in a pipe of uniform circular cross section.

To this end, we must solve the Navier-Stokes equation for incompressible fluids, i.e.,

$$\rho \left(\frac{\partial \vec{v}}{\partial t} + (\vec{v} \cdot \nabla)\vec{v}\right) = -\nabla p + \nabla \cdot \sigma \tag{8}$$

$$\nabla \cdot \vec{v} = 0 \tag{9}$$

with σ given by the constitutive Eq. (12). This is a highly nonlinear set of coupled equations. Hence, it turns out to be rather difficult to carry out an analytical treatment of any flow property of a viscoelastic fluid.

Henceforth, we shall consider only flows in which the Weissenberg and Reynolds numbers are very small. The latter means that the convective term $(\vec{v} \cdot \nabla)\vec{v}$ in the Navier-Stokes equation is negligible. With these assumptions, the set of governing equations is determined by

$$\rho \frac{\partial \vec{v}}{\partial t} = -\nabla p + \nabla \cdot \sigma, \tag{10}$$

$$\nabla \cdot \vec{v} = 0 \tag{11}$$

and

$$\sigma + \lambda \frac{\partial \sigma}{\partial t} = 2\eta_0 \left(\mathbf{D} + \lambda \frac{\eta_s}{\eta_0} \frac{\partial \mathbf{D}}{\partial t}\right). \tag{12}$$

A more precise discussion of the above assumptions comes in the following. This type of flow occurs, typically, under the influence of a reciprocating piston located at one end of a pipe of circular cross-section [1, 5, 7] and references therein. We assume that the pipe length is much larger than its radius and we shall study the flow very far from the moving piston. There, under the previous assumptions, the flow can be described by the component of the velocity

along the pipe axis. Moreover, owing to the incompressibility assumed and symmetries involved, the velocity only depends on the distance to the pipe axis, $\vec{v} = v_z(r,t)\mathbf{e_z}$ and the pressure only varies in the longitudinal direction $\nabla p = \frac{dp(z,t)}{dz}\mathbf{e_z}$. With these assumptions, the pressure gradient must be constant along the pipe.

Then, the convective term in the Navier-Stokes equation vanishes identically leading to

$$\rho\frac{\partial v_z(r,t)}{\partial t} = -\nabla p + \nabla\cdot\sigma. \tag{13}$$

Taking the divergence of both sides of Eq. (12), from the definition of **D**, and bearing in mind the expression for the velocity, it can be obtained $2\nabla\cdot\mathbf{D} = \nabla^2 v_z$. These assumptions lead (12) to

$$\nabla\cdot\sigma + \lambda\frac{\partial\nabla\cdot\sigma}{\partial t} = \eta_o\left(\nabla^2 v_z + \lambda_r\frac{\partial\nabla^2 v_z}{\partial t}\right), \tag{14}$$

where $\lambda_r = \lambda\frac{\eta_s}{\eta_0}$ is a constant with dimensions of time.

If we derive with respect to time, multiply by λ both sides of (13) and substituting the term $\lambda\frac{\partial\nabla\cdot\sigma}{\partial t}$ from (14), we obtain

$$\lambda\rho\frac{\partial^2 v_z(r,t)}{\partial t^2} + \rho\frac{\partial v_z(r,t)}{\partial t} = -\lambda\frac{\partial\nabla p}{\partial t} + \eta_o\left(\nabla^2 v_z + \lambda_r\frac{\partial\nabla^2 v_z}{\partial t}\right) \tag{15}$$

Let us now refer all linear dimensions to the pipe radius R, time to $\frac{R^2}{\nu_o}$, and the velocity to $\frac{KR^2}{\nu_o}$ where K is the amplitude of the pressure gradient divided by the fluid density and ν_o is its kinematic viscosity at steady motion.

Thus, it can be obtained that

$$A\frac{\partial^2\Lambda(\xi,\tau)}{\partial\tau^2} + \frac{\partial\Lambda(\xi,\tau)}{\partial\tau} = \nabla^2\Lambda(\xi,\tau) + A\frac{\eta_s}{\eta_o}\frac{\partial\nabla^2\Lambda}{\partial\tau} - \left(A\frac{\partial\nabla p}{\partial\tau} + \nabla p\right), \tag{16}$$

where $A = \frac{\lambda\nu_0}{R^2}$ denotes the inverse of Deborah number, τ, ξ, and $\Lambda(\xi,\tau)$ denote the dimensionless time, radial coordinate and velocity, respectively.

Fourier transformation of the latter equation leads to

$$\frac{1}{\xi}\frac{\partial}{\partial\xi}\left(\xi\frac{\partial\widetilde{\Lambda}(\xi,\alpha)}{\partial\xi}\right) + i\alpha\frac{1-i\alpha A}{1-i\alpha A\eta'}\widetilde{\Lambda}(\xi,\alpha) = \frac{1-i\alpha A}{1-i\alpha A\eta'}\frac{\partial\widetilde{p}(\alpha)}{\partial z} \tag{17}$$

where $\alpha = \frac{\omega R^2}{\nu_o}$. This number is the ratio between inertia and viscosity forces, so it can be regarded as a Reynolds number for non-steady flows. $\widetilde{\Lambda}(\xi,\alpha)$ and $\frac{\partial\widetilde{p}(\alpha)}{\partial z}$ denote the Fourier transform of the velocity and pressure gradient, respectively. Hereafter, we shall drop the upper hat and the dependence on α will indicate the Fourier Transform, unless otherwise noted. In (17) $\eta' = \frac{\eta_s}{\eta_o}$ is the viscosity ratio.

To obtain the velocity field, boundary conditions must be added, namely, the no-slip condition at the wall and the fact that the velocity must remain finite at the pipe axis.

Then it follows for the velocity

$$\Lambda(\xi,\alpha) = \frac{1}{i\alpha}\left(1 - \frac{J_0(\beta'\xi)}{J_0(\beta')}\right)\frac{dp(\alpha)}{dz}, \tag{18}$$

$$\beta'^2(\alpha) = i\alpha\frac{1-i\alpha A}{1-i\alpha A\eta'} \tag{19}$$

If we make $\eta' \to 0$ in the above equation, the same result as for the Maxwell model is obtained, see [4, 5, 15]. In addition, making also $A \to 0$, the Newtonian behavior is recovered, see [1].

Now, following the same procedure as in [4, 5, 7], we shall calculate the average velocity over a cross section. Thus,

$$\langle\Lambda(\xi,\alpha)\rangle_\xi = \left\langle\frac{1}{i\alpha}\left(1 - \frac{J_0(\beta'\xi)}{J_0(\beta)}\right)\right\rangle_\xi\frac{dp(\alpha)}{dz}, \tag{20}$$

where the symbol $\langle(...)\rangle_\xi$ denotes the spatial average over the cross-section of the quantity inside brackets.

From the above expression, it can be inferred that the total flux is proportional to the pressure gradient. This resembles Darcy's Law in frequency domain. Then, we define the dynamic permeability as

$$K(\alpha) = -R^2\frac{\langle\Lambda(\xi,\alpha)\rangle_\xi}{dp(\alpha)/dz} \tag{21}$$

3.2 Comparison with Experimental Results

To compare with experimental results, we shall, as in [5], define a local dynamic response (**LDR**) as follows:

$$\kappa(\alpha) = -R^2\frac{\Lambda(0,\alpha)}{dp(\alpha)/dz} \tag{22}$$

In [5], a detailed experimental study of the dynamic response of a Newtonian fluid, the Glycerol, and a viscoelastic fluid, *CPyCl/NaSal* solution, under an oscillating pressure gradient was performed. Measurements of fluid particles velocity and the root mean square velocity V_{rms} were made inside a straight vertical cylinder with circular cross section.

In [5], the pressure gradient was described by

$$\frac{dp(t)}{dz} = \rho z_0 w^2 sin(\omega t) \tag{23}$$

in which z_0 represents the piston displacement amplitude equal to 0.8 mm. Thus the experimental value of the (**LDR**) $\kappa^e(\alpha)$ is defined in [5] as

$$\kappa^e(\alpha) = \eta_0\frac{v_{rms}}{dp_{rms}/dz} \tag{24}$$

Hence, since the velocity in the experiment varies sinusoidally, the above expression assumes the form

$$\kappa^e(\alpha) = \eta_0 \frac{v_0}{\rho z_0 w^2} \tag{25}$$

where v_0 denotes the amplitude of the velocity oscillation.

Thus, the absolute value of (22) can be compared directly with (25), provided the velocity and the pressure gradient are sinusoidals.

Theoretical results given by the Maxwell model [5, 7, 15], reproduce quite well the values of α at which the peaks in the **LDR** of the *CPyCl/NaSal* solution are observed. However, the predicted relative amplitude deviates from the experimental results. In the Maxwell model, the relative amplitude is larger than the experimental values, and this model also fails in predicting the decrease of the **LDR** observed experimentally. In [5], it is speculated that these differences might be due to nonlinear phenomena that occur in the *CPyCl/NaSal* solution as well as to compressibility effects that could take place when the frequency is increased. A thorough discussion about the influences of compressibility and nonlinearities in the mechanical properties of the viscoelastic solution is presented below.

Let us now compare our presents derivations with the experimental data reported in [5, 7], and with the corresponding calculations for the Maxwell model, also reported in these references.

In Fig. 1, the comparison of our calculation with experimental results is shown. As in [5], we plot the LDR scaled by its value at steady motion versus α. The theoretical curve exhibits a good agreement with experiments. The curve shape is quite similar for values of α in the range of 0.4 to 1 and only slightly differs in the amplitude of the response. We can see that the decrease in the

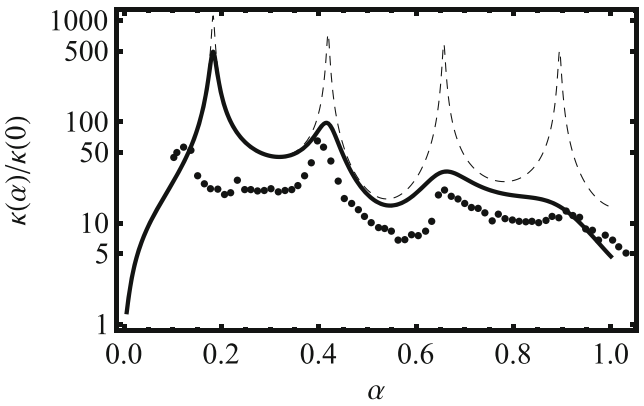

Fig. 1 Comparison between the Maxwell and Oldroyd-B models with experiments for the *CPyCl/NaSal* solution performed in [5]. The *dashed line* is the absolute value of $\kappa(\alpha)$ predicted by the Maxwell model. The *continuous black line* is the result for the Oldroyd-B model with the same value of A=173.71 and $\eta_0 = 60 Pa \cdot s$. The solvent viscosity is $\eta_s = 0.08 Pa \cdot s$, leading to $\eta' = 0.8 \cdot 10^{-3}$. Experimental values are shown by points

dimensionless LDR observed experimentally is quite well reproduced. This allows us to infer that as α increases, the purely Newtonian component becomes stronger and dissipative effects are more evident. In fact, this can be predicted from Eq. (12). From the definition of α and assuming that the viscosity η_o does not depend on the velocity gradients, an increase in α leads to an increase in the number $\omega\lambda\frac{\eta_s}{\eta_0}$. If the latter number is much larger than unity, we have in Eq. (12)

$$\|\lambda\frac{\partial\sigma}{\partial t}\| \gg \|\sigma\| \qquad \|\lambda\frac{\eta_s}{\eta_0}\frac{\partial D}{\partial t}\| \gg \|D\|. \tag{26}$$

Therefore, in this limit, we have for the stress in the viscoelastic solution

$$\sigma \sim 2\eta_s D \tag{27}$$

Hence, the solution behaves in this case as a Newtonian liquid. Moreover, from the above arguments, we see that the Newtonian factor becomes stronger as the number $\omega\lambda\frac{\eta_s}{\eta_0}$ is increased. This is a significant difference from Maxwell liquids, whose behavior is similar to a Hookean solid when $\omega\lambda \gg 1$ [11]. Thus, there is a transition from viscoelastic to purely dissipative (Newtonian) dynamics of oscillating flows of Oldroyd-B fluids. We stress the fact that the relevant parameter for this transition is the number $\omega\lambda\frac{\eta_s}{\eta_0}$, which does not depend on the geometrical properties in which the fluid is confined. Another noteworthy observation is that neither nonlinearities nor compressibility effects have been taken into account. Nevertheless, in Fig. 1, it can be seen that both models exhibit similar behavior and overestimate the relative amplitude of the LDR at low frequencies.

The curve for the Oldroyd-B model was obtained using the relaxation time $\lambda = 1.9$ s, and the viscosity at steady flow, $\eta_0 = 60 Pa \cdot s$ reported in [5, 18]. Besides, the value of the solvent viscosity which provides the best fit to the experimental data was $\eta_s = 0.08 Pa \cdot s$. This value is approximately 80 times larger than the water viscosity, which is the solvent of the *CPyCl/NaSal* 60/100 solution. Thus, the Newtonian factor considered here within the Oldroyd-B model must be thought as a contribution leading to an effective viscosity larger than the water viscosity. This result might be due to the fact that *CPyCl/NaSal* 60/100 solution is not very dilute [18], whereas the Oldroyd-B model is valid only for dilute polymer solutions [14, 19], where the hydrodynamic interactions are neglected. For highly concentrated solutions, disturbances of the solvent velocity field generated by the motion of the polymer molecule (coil) affects the drag force on the neighboring coils. As a consequence, the total drag force is larger than the total force that would be produced if the solution were very dilute. So, using in this case, the Oldroyd-B model leads to consider effective values of the parameters involved in the model.

Another quantity reported in [5] is the root mean square value of the velocity at the pipe axis. Since, as mentioned before, the pressure gradient varies sinusoidally, we assume that the velocity field has the form

$$v_z(r,t) = Im(\phi(r)e^{i\omega t}) \tag{28}$$

Substitution of Eqs. (28) and (23) in (15) leads to an ordinary differential equation for $\phi(r)$[1], whose vanishing solution at the pipe wall, $r = R$, is given by

$$\phi(r) = \frac{z_0\omega}{i}\left(1 - \frac{J_0(\beta r)}{J_0(\beta R)}\right), \tag{29}$$

$$\beta^2 = -i\frac{\omega}{\nu_0}\left(\frac{1+i\omega\lambda}{1+i\omega\lambda\eta_s/\eta_0}\right). \tag{30}$$

From Eqs. (29) and (28), we have for the velocity

$$v_z(r,t) = H_0(r,\omega)sin(\zeta + \omega t) \tag{31}$$

where $H_0(r,\omega) = \sqrt{Re^2(\phi(r)) + Im^2(\phi(r))}$ and $\zeta = arctan\frac{Im(\phi(r))}{Re(\phi(r))}$

Therefore, the root mean square of the velocity can be calculated as follows:

$$V_{rms} = \frac{H_0(r,\omega)}{\sqrt{2}} \tag{32}$$

The next figure shows a comparison between predictions of the Oldroyd-B model and experimental values for the root mean square velocity at $r = 0$. We can observe that the Oldroyd-B model can reproduce accurately the frequencies at which peaks of the root mean square velocity are observed. Moreover, the curve shape is well reproduced for frequencies above 4 Hz. These agreements reinforce the fact that the pure Newtonian contribution of the solvent is very important in the dynamic behavior of the *CPyCl/NaSal* solution.

As a natural extension of the experiments reported in [5], in [7] the velocity profiles were measured at different heights from the piston, exploring the behavior of the velocity throughout the whole cross-section of the pipe. In the range of frequencies covered in the experiments in the latter reference, we have found that there is no significant differences among the velocity profiles predicted by the Maxwell and linear Oldroyd-B models, given by equations (1) in Ref. [7] and (31) in our present derivations, respectively. More precisely, we have compared the velocity profiles for both models in the frequencies reported in figures 8, 14, and 15 of [7]. We have used for the comparison the same values of the parameters as for the fit made in Figs. 2 and 1. In both cases, the velocity profiles are quite similar, namely, the number of quiescent flow points is the same and they are located roughly in the same position as can be seen in

[1]This is the same equation obtained for the Fourier transform of the velocity

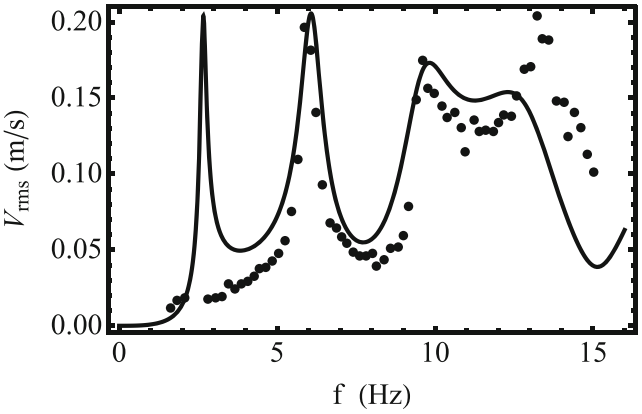

Fig. 2 Superposition of the root mean square velocity predicted by the Oldroyd-B model at the pipe axis represented by the *continuous black line*, (32) evaluated at $r = 0$, with the experimental values reported in [5], shown by points in the graph. A better fit than the one provided by the Maxwell model is exhibited here for frequencies higher than 4 Hz. The curve shape is quite well reproduced, although still the linear Oldroyd-B model overestimates the response amplitude. The values of density and viscosity of the *CPyCl/NaSal* solution were used [5, 18]. The solvent viscosity that provides the fit is equal to 0.08 $Pa \cdot s$

Fig. 3, only the amplitude of the velocity at the pipe axis is lower for the Oldroyd-B model. A comparison for a wider range of frequencies can be found in [2]. It is worth noting that main differences appear at higher frequencies. At such frequencies, as explained above, the viscous transport of momentum has a considerable effect on the entire flow by smoothing out all the small scales inhomogeneities of the velocity field. As a consequence, for sufficiently high driving frequency, a flow with boundary layer characteristics is formed in which large velocity gradients are only found near the tube wall. In that sense, more measurements of the entire velocity field at high frequencies, keeping a laminar regime, are needed in order to elucidate whether this prediction is correct or not for the viscoelastic solution in question.

However, disagreements are evident for both linear models at low frequencies with experiments and there is a persistent overestimation of the response amplitude in the range of frequencies covered by the experiments. As observed more recently in [6], due to nonlinear rheological properties of the complex fluid (disregarded in our present derivations), there are instabilities that arise as the driving frequency and/or amplitude of the forcing are increased. The origin of such instabilities might lie in the anisotropies in the stress tensor field created by the basic shear flow structure [17]. With this thought in mind, let us now examine a little more closely the Oldroyd-B constitutive Eq. (7) in the case of pure shear flows.

Let us first note that in such flows the velocity gradient tensor satisfies, besides the incompressibility condition $TrD = 0$, an additional constraint $(\nabla v)_{ij}(\nabla v)_{jk} = 0$ [16]. Moreover, the operator $\vec{v}\cdot\nabla$ vanishes identically, as

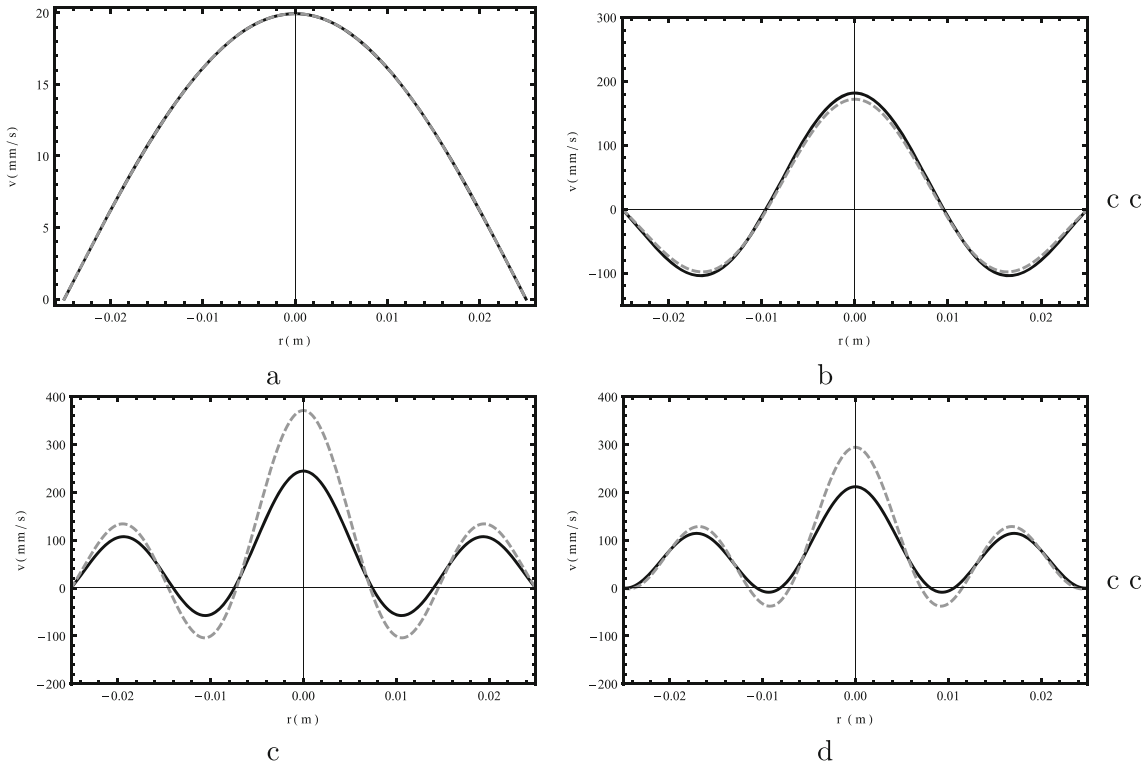

Fig. 3 Comparison of the velocity profiles predicted by the Maxwell model (*dashed line*) and Oldroyd-B model (*continuous line*) at a driving frequency of **a** 2 Hz, **b** 6.5 Hz, **c** 10 Hz, and **d** 11.5 Hz. The value of the solvent viscosity for the Oldroyd-B model used was $\eta_s = 0.08 Pa \cdot s$, as in the fit used in Figs. 1 and 2. The remainder parameters are the same as in [7]. The graphs were obtained at the instant in which the maximum velocity at the pipe axis was reached. In **b**–**d**, we can see that the number of quiescent point flows are the same and are located in the same position roughly. We can also note in **c**, **d** that as the driving frequency is increased, the influence of viscosity becomes more significant and then the velocity at the pipe axis is lower for Oldroyd-B liquids, and consequently the velocity gradient are also lower than the predicted values for the Maxwell model near the pipe axis

mentioned above. Then, it follows for the upper convected derivative of the velocity gradient tensor

$$\frac{\delta D}{\delta t} = \frac{\partial D}{\partial t} - 2(\nabla v)^t \cdot \nabla v. \tag{33}$$

With the latter result, the Oldroyd-B constitutive equation can be written as

$$\sigma + \lambda \frac{\partial \sigma}{\partial t} - \lambda \left[\sigma \cdot \nabla v + (\nabla v)^t \cdot \sigma\right] = \eta_0 \left(\mathbf{D} + \lambda \frac{\eta_s}{\eta_0} \left[\frac{\partial D}{\partial t} - 2(\nabla v)^t \cdot \nabla v\right]\right). \tag{34}$$

The effects (assumed weak) of the nonlinear terms can be assessed by a perturbation procedure. Indeed, an expansion of the stress tensor in terms of the Weissenberg number [2] $\sigma = \sigma_0 + (Wi)\sigma_1 + O(Wi^2)$ substituted in Eq. (35) gives to zero and first order

$$\sigma_0 + \lambda \frac{\partial \sigma_0}{\partial t} = 2\eta_0 (\nabla v + (\nabla v)^t) \tag{35}$$

and

$$\sigma_1 + \lambda \frac{\partial \sigma_1}{\partial t} = \eta_s \frac{\partial (\nabla^* v^* + (\nabla^* v^*)^t)}{\partial t} - 2\eta_s \gamma_o \nabla^* v^* \cdot (\nabla^* v^*)^t + \left[\sigma_0 \cdot \nabla^* v^* + (\nabla^* v^*)^t \cdot \sigma_0\right], \tag{36}$$

respectively. In Eq. (36), the quantity $\nabla^* v^*$ denotes a dimensionless velocity gradient tensor defined by the relation $\nabla v = \gamma_o \nabla^* v^*$. In the particular case we are concerned with, in which the only nonvanishing component of the velocity gradient (of the basic flow) is $\nabla v_{rz} = \frac{\partial v_z}{\partial r}$, from Eqs. (35) and (36), we can see that the last two terms in the r.h.s of Eq. (36) are responsible for the appearance of a normal stress σ_{zz}. This shear-induced anisotropy in the stress tensor is a nonlinear effect which is absent from the corresponding Newtonian flow and has been disregarded in our present derivations. Due to this anisotropy, if the fluid suffered a perturbation of large enough amplitude it would have a transition to a sort of weakly turbulent state [17]. This was indeed observed in [6]. In such a case, our analytical treatment breaks down. From the analysis of the order

[2] In oscillating flows, we can define the Weissenberg number as $Wi = \lambda \gamma_o$, where γ_o is the root mean square of a characteristic velocity gradient. The latter quantity can be defined, as in [6], as the ratio between the velocity of the piston and the distance between the pipe axis and the first quiescent radial position of the flow

of magnitudes of the terms involved in the equations resulting from our perturbation procedure, we can note that shear stresses becomes much larger than the normal ones when the following condition is satisfied $\frac{\gamma_o}{\omega} \ll 1$[3]. In contrast, when $\frac{\gamma_o}{\omega}$ becomes of the order of unity or even larger, the normal stresses are significant and the fluid might develops secondary unstable motions. The analysis of figure 20 of reference [6] confirms our assertion. Also, from the analysis of Fig. 3, we can observe that for a given amplitude of the piston the fluid experiences larger flow rates as the resonance frequencies are increased. This is in qualitative agreement with the results reported in [6]. We stress the fact that in deriving these results, we did not consider the shear thinning behavior of the viscoelastic solution. When the condition $\frac{\gamma_o}{\omega} \ll 1$ is fulfilled, the replacement of the upper-convected time derivative by the local time derivative is a good approximation. It is interesting try to corroborate this criterion in detail for different types of complex fluids.

As for the compressibility, from Fig. 2, the highest velocity in the fluid v_m is approximately equal to 0.3 m/s. Then, since the speed of sound in liquids is of order $v_s \sim 10^3$m/s, we have for the Mach number $M \sim 10^{-4}$. At such low Mach numbers, compressibility effects must be weak [1, 21], so the compressibility does not seem to be an important factor in the decay of the peaks. Let us present in the next section a detailed derivation that confirms this assertion.

4 Influence of Compressibility

As mentioned above, at these low Mach numbers, compressible effects must be weak. Nonetheless, in this section, we will be aimed at modeling the problem of sound waves propagation in viscoelastic fluids flowing inside pipes. The influence of viscoelastic properties in sound wave propagation phenomena in infinite fluids and in wall-bounded flows (inside straight pipes) has already been addressed in [20] and [2], respectively.

Let us first revisit the stress modeling problem in compressible fluids. It is well known (see for instance, [22] and [23]) that the motion in the neighborhood of any point consists of the superposition of:

1 A uniform translation,
2 A pure strain motion characterized by the rate of strain tensor $D = \nabla v + (\nabla v)^t$, which can be decomposed itself into an isotropic expansion (contraction) in which the rate of extension of all line elements is $\frac{1}{3}\nabla \cdot v$ and a straining motion without changes of volume characterized by $D_{ij} - \left(\frac{1}{3}\nabla \cdot v\right)\delta_{ij}$, and
3 A rigid body rotation with local angular velocity given by $\frac{\nabla x u}{2}$

We shall restrict ourselves, as in previous sections, to flows in which the Weissenberg number is sufficiently small so we shall not consider shear-induced anisotropy in elastic stresses. Besides, we can assume a linear relationship between normal stresses and velocity derivatives by considering small oscillations of fluid particles in the wave motion. Moreover, as in the case of incompressible viscoelastic solutions, we shall consider that the stresses generated by the straining motion without changes in volume and by isotropic expansion relax on time scales λ_1 and λ_2, respectively. Then, the constitutive (linear) equations for the extraviscoelastic stresses may be written as follows:

$$\sigma_1^e + \lambda_1 \frac{\partial \sigma_1^e}{\partial t} = \eta_1 \mathbf{D} - \frac{2}{3}\eta_1 \nabla \cdot \vec{v}\, \mathbf{I}, \tag{37}$$

and

$$\sigma_2^e + \lambda_2 \frac{\partial \sigma_2^e}{\partial t} = \eta_2 \nabla \cdot \vec{v}\, \mathbf{I}, \tag{38}$$

where $\mathbf{I}$ is the identity tensor of rank 2. The total viscoelastic stress σ is obtained by summing σ_1^e and σ_2^e.

At this point, it is useful to note that for times larger than λ_1 the trace of the total viscoelastic stress satisfies the differential equation

$$Tr\sigma + \lambda_2 \frac{\partial Tr\sigma}{\partial t} = 3\eta_2 \nabla \cdot \vec{v}\, \mathbf{I}, \tag{39}$$

which coincides with the postulated equation for the trace of the stress tensor in [20] when the displacements of fluid particles in the wave are small compared with the wave length or equivalently, when the velocity of fluid particles in the wave is small compared with the velocity of sound.

The formal solution for the total viscoelastic stress can be written as follows:

$$\sigma = \int_0^\infty ds[G(s)\mathrm{D}(t-s) + \{K(s) - 1/3G(s)\}\mathbf{I}Tr\mathbf{D}(t-s)], \tag{40}$$

in which

$$G(t) = (\eta_1/\lambda_1)e^{-t/\lambda_1}$$

and

$$K(t) = (\eta_2/\lambda_2)e^{-t/\lambda_2}$$

denote the relaxation functions of shear and normal stresses, respectively.

Substituting this formal solution into the momentum balance equation leads to

$$\rho\left((\vec{v}\cdot\nabla)\vec{v} + \frac{\partial \vec{v}}{\partial t}\right) = -\nabla p + \eta_s \nabla^2 \vec{v} + \int_0^\infty ds[G(s)\nabla^2 \vec{v} + A(s)\nabla(\nabla \cdot \vec{v})], \tag{41}$$

where $A(s) = K(s) + \frac{1}{3}G(s)$.

[3] Note that $\frac{\gamma_o}{\omega}$ coincides with the definition of the control parameter χ of (6) of reference [6].

Since we are considering that the velocity of fluid particles is small compared with the velocity of sound, we can neglect the term $(\vec{v}\cdot\nabla)\vec{v}$ in the above equation. For the same reason, the relative changes in the fluid pressure and density should be small. Hence, we can write the latter magnitudes as follows:

$$p = p_o + p' \qquad \rho = \rho_o + \rho',$$

where p_o and ρ are the values of the pressure and density, respectively, in the unperturbed state, while the primed quantities refer to the oscillating part.

The equation of continuity in the linear approximation can be written as follows:

$$\frac{\partial \rho'}{\partial t} + \rho_0 \nabla \cdot \vec{v} = 0. \tag{42}$$

We may also note, since we are considering small deviations from the state of equilibrium, that the changes in the entropy s are of second order of smallness [21]. In this approximation, to the first order of accuracy, we have that changes in the fluid pressure are only caused by variations in the fluid density. Then we can write $p \approx p(\rho)$. Hence the small variations of p' are related to changes in ρ' in the following way

$$p' = \left(\frac{\partial p'}{\partial \rho}\right)_s \rho' = c^2 \rho', \tag{43}$$

where c is the speed of sound.

After substituting for ρ' according to the above equation in (42) we obtain

$$\frac{\partial p'}{\partial t} + c^2 \rho_0 \nabla \cdot \vec{v} = 0. \tag{44}$$

With the Eqs. (44) and (42) for the four unknowns p' and $\vec{v}$, we are able to completely describe the sound wave. Moreover, in order to express the two unknowns in term of one of them, it is convenient to take the divergence of both sides of Eq. (42) and take the time derivative of Eq. (44). Then, it can readily be obtained the following equation describing the small oscillations of pressure, which was also derived in [20]

$$\rho_0 \frac{\partial^2 p}{\partial t^2} = K_x \nabla^2 p + \eta_s \frac{\partial}{\partial t}\nabla^2 p + \int_0^\infty ds M(s) \frac{\partial}{\partial t}\nabla^2 p(t-s), \tag{45}$$

in which $K_x = \rho_o c^2$ is the compressibility modulus and $M(s) = K(s) + \frac{4}{3}G(s)$. Here and henceforward, we shall omit the prime symbol to the small variations of pressure.

With the same assumptions as in Section 3.1 concerning the flow geometry, we shall consider that the velocity field in the sound wave can be described in terms of its component along the z-axis, i. e.,

$$\vec{v} = v_z(r, z, t)\mathbf{e_z}. \tag{46}$$

As a consequence of the latter, the pressure will vary only along the pipe axis and will be constant along the cross section.

$$p = p(z). \tag{47}$$

A noteworthy observation is that the velocity must depend on z, owing to the compressibility, which represent the main difference with the flow of an incompressible liquid.

Let us seek a solution for Eqs. (44) and (42) in the form of a plane wave,

$$v_z(r, z, t) = Re[\phi(r)e^{i(kz-wt)}] \qquad p = Re[P_0 e^{i(kz-wt)}]. \tag{48}$$

Substitution of the above expression for the pressure in Eq. (44) leads to the dispersion relation

$$k^2 = \left(\frac{w}{c_x}\right)^2 \left[1 + \frac{iw\eta_0}{\rho_0 c_x^2}\left(\frac{\eta_s}{\eta_0} + \frac{4}{3}\frac{\eta_1}{\eta_0}\frac{1}{1-iw\lambda} + \frac{\eta_2}{\eta_0}\frac{1}{1-iw\lambda}\right)\right]^{-1}. \tag{49}$$

Similarly, after substitution of the expression for the velocity and the pressure itself in (42), we obtain an ordinary differential equation for $\phi(r)$

$$\nabla_r^2 \phi(r) + \left(\frac{i\omega\rho_0}{\eta_0}\frac{1-i\omega\lambda}{1-i\omega\lambda\eta'} - \frac{k^2\left(\frac{4}{3}(1-\eta') + \eta_2'\right)}{i\omega\lambda\eta'}\right)\phi(r) = -i\frac{kP_0}{\eta_0}\frac{1-i\omega\lambda}{1-i\omega\lambda\eta'}, \tag{50}$$

in which $\nabla_r^2 = \frac{1}{r}\frac{\partial}{\partial r}\left(r\frac{\partial}{\partial r}\right)$, $\eta' = \frac{\eta_s}{\eta_0}$ and $\eta_2' = \frac{\eta_2}{\eta_0}$.

Solving the equation for $\phi(r)$, we obtain for the velocity

$$v_z(r, z, t) = -\frac{ikP_0 e^{i(kz-wt)}}{i\omega\rho_o - \frac{k^2\eta_0}{1-i\omega\lambda}\left(\frac{4}{3}(1-\eta') + \eta_2'\right)}\left(1 - \frac{J_0(\beta_c r)}{J_0(\beta_c R)}\right). \tag{51}$$

In the above expression, it has been defined

$$\beta_c^2 = \left(\frac{i\omega\rho_0}{\eta_0}\frac{1-i\omega\lambda}{1-i\omega\lambda\eta'} - \frac{k^2\left(\frac{4}{3}(1-\eta') + \eta_2'\right)}{i\omega\lambda\eta'}\right).$$

Noting that $\frac{dp}{dz} = ikP_0 e^{i(kz-wt)}$, we can conveniently rewrite the above equation as

$$v_z(r, z, t) = -\frac{1}{i\omega\rho_o - \frac{k^2\eta_0}{1-i\omega\lambda}\left(\frac{4}{3}(1-\eta') + \eta_2'\right)}\left(1 - \frac{J_0(\beta_c r)}{J_0(\beta_c R)}\right)\frac{\partial p}{\partial z}, \tag{52}$$

which resembles the corresponding velocity for the incompressible case (18).

Hence, defining the local dynamic permeability as in Section 3.2 by

$$\kappa_c = \frac{-\eta_0 v_z(0,z,t)}{\frac{\partial p}{\partial z}}, \tag{53}$$

and referring the frequency to $\frac{\nu_0}{R^2}$, the inverse of the characteristic time of vorticity diffusion due to viscosity is obtained as follows:

$$\kappa_c(\alpha) = -\frac{R^2}{i\alpha - \varepsilon_c}\left(1 - \frac{1}{J_0(\beta_c')}\right), \tag{54}$$

in which

$$\varepsilon_c = \frac{\left(\frac{\alpha}{Re_x}\right)^2\left[\frac{4}{3}(1-\eta') + \eta_2'\right]}{(1-i\alpha A)\left(1 + i\frac{\alpha}{Re_x^2}\left(\left[\frac{4}{3}(1-\eta') + \eta_2'\right]\frac{1}{1-i\alpha A} + \eta'\right)\right)} \tag{55}$$

and

$$\beta_c'^2 = (i\alpha - \varepsilon_c)\frac{1 - i\alpha A}{1 - i\alpha A\eta'} \tag{56}$$

In the above expressions, it has been used $Re_x = \frac{c_x R}{\nu_o}$. The dimensionless numbers A and α are defined in the same way as before.

In experiments with the $CPyCl/NaSal$ solution, the range of frequencies covered kept the number α in the range $0 < \alpha < 1$. Estimating that the speed of sound in the solution is $c_x \sim 10^3$m/s, leads to $Re_x \sim 10^3$ and thus $\left(\frac{\alpha}{Re_x}\right)^2 \sim 10^{-6}$. Let us also assume that $\eta_2' \sim 1$ (see [21]) and that relaxation times of shear and normal stresses are of the same order of magnitude. Evaluating the remainder parameters as in the incompressible case, we obtain that $Abs(\varepsilon_c) \ll 1$ leading to $\beta_c'^2 \cong \beta'^2$. Thus, we reach the conclusion that for weakly compressible flows, the **LDR** matches almost perfectly the corresponding incompressible flow. We can see very slight differences in the values of frequencies at which peaks are observed as well as in the amplitude of the **LDR** provided only that $\frac{\alpha}{Re_x} \sim 1$ [2].

5 Conclusions

In this paper, we have discussed some non-Newtonian effects of an Oldroyd-B fluid under oscillating pressure gradient. A relation was derived between flux velocity and pressure gradient in frequency domain that resembles Darcy's Law. An analytical expression was given for the dynamic permeability in terms of dimensionless parameters, which are the number α that represents the ratio between the inertia and viscosity forces; the inverse of Deborah's number, which is the ratio between characteristic times of viscous effects and elastic ones; and the number $\omega\lambda\frac{\eta_s}{\eta_0}$, which determines the differences between the Oldroyd-B and Maxwell models. Moreover, our calculations have predicted a transition from a Non-Newtonian (viscoelastic) to purely Newtonian behavior in the dynamics of viscoelastic solutions when the condition $\omega\lambda\frac{\eta_s}{\eta_0} \gg 1$ is satisfied. This transition is therefore independent of the flow geometry, i.e., it has a universal character. We have found good agreement between the linear Oldroyd-B model predictions for the local dynamic response, as well as for the root mean square velocity at the pipe center, and the corresponding experimental data, shown in Figs. 1 and 2, respectively.

This suggests that the dissipative factor, present in Oldroyd-B fluids, may be responsible for the decrease of the local dynamic response observed in experiments [5]. However, these good agreements are obtained when the solvent viscosity used in the fitting is considered as an increased coefficient owing to the possible fact that due to high concentrations of the viscoelastic solution, disturbances of the solvent velocity field generated by the motion of the polymer molecule (coil) affects the drag force on the neighboring coils. Consequently, the solvent viscosity is actually used here as a free parameter. The very small Mach numbers at which experiments were made indicate that compressibility effects can be neglected.

Our derivations confirmed that, given the experimental conditions, weakly compressible effects will not contribute to any significantly change in the local dynamic response of the fluid compared with the incompressible result. By means of a perturbation procedure to the Oldroyd-B equation, we derived a criterion for the onset of instabilities in shear oscillating flows that was experimentally verified in [6]. According to this criterion, if the number $\frac{\gamma_o}{\omega}$ were of order or larger than unity, the normal stresses would make unstable any finite perturbation to the basic parallel shear flow. This kind of instabilities and the shear thinning behavior of the viscelastic solution may be the origin of the disagreements between the results of our present derivation for the linear Oldroyd-B model.

Acknowledgments We are grateful to the anonymous reviewer who kindly pointed us reference [6] containing very useful discussions and results for the study of phenomena involved in the present study.

References

1. H. Schlichting. *Boundary Layer Theory* (Mc Graw-Hill Book Company, 1973)
2. A.H. García, O.-S. Costa, Cuban J. Phys. **28**(1) (2011)
3. A.H. García, Diploma thesis Waves in Viscoelastic Media (2009)
4. D. Tsiklauri, I. Beresnev, Phys. Rev. E. **046304**, 63 (2001)
5. J.R. Castrejón-Pita, J.A. del Río, A.A. Castrejón-Pita, G. Huelsz, Phys. Rev. E. **046301**, 68 (2003)
6. M. Torralba, A.A. Castrejón-Pita, G. Hernández, G. Huelsz, J.A. del Río, J. Ortín, Phys. Rev. E. **056307**, 75 (2007)
7. M. Torralba, J.R. Castrejón-Pita, A.A. Castrejón-Pita, G. Huelsz, J.A. del Río, Phys. Rev. E. **016308**, 72 (2005)
8. J.A. del Río, M. López de Haro, S. Whitaker, Phys. Rev. E. **58**, 6323 (1998)

9. J.G. Oldroyd, On the formulation of rheological equations of state. Proc. R. Soc. **A200**, 523–541 (1950)
10. Skelland. *Non-Newtonian Flow and Heat Transfer* (Wiley, New York, 1967)
11. R.B. Bird, W.E. Stewart, E.N. Lightfoot. *Transport Phenomena*, 2nd Edn (Wiley, 2002)
12. S.J. Muller, R.G. Larson, E.S.G. Shaqfeh. Rheol. Acta. **28**, 499–503 (1989)
13. G. Prilutski, R.K. Gupta, T. Sridhar, M.E.J. Ryan, Non-Newton. Fluid Mech. **12**, 233–41 (1983)
14. R.G. Larson. *The Structure and Rheology of Complex Fluids* (Oxford University Press, 1999)
15. J.A. del Río, J.R. Castrejón-Pita, Revista Mexicana de Fí. **49**(1), 74–85
16. S.L. Victor, A. Pomyalov, I. Procaccia, V. Tiberkevich, Phys. Rev. E. **016305**, 71 (2005)
17. N. Alexander, Wim van Saarlos Phy. Rep. **447**, 112–143 (2007)
18. J.F. Berret, J. Apell, G. Porte, Langmuir. **9**, 2851 (1993)
19. S. Berti, Ph.D. Thesis Non-Newtonian turbulence: viscoelastic fluids and binary mixtures (2006)
20. O.S. Costa, A.V. Vázquez, J.M. Antuña, Brazilian Journal of Physics, vol. 27, no. 3
21. L.D. Landau, E.M. Lifshitz. *Fluid Mechanics* (Pergamon Books Ltd., 1987)
22. G.K. Batchelor. *An Introduction to Fluid Dynamics* (Cambridge University Press, 2000)
23. A.J. Chorin, J.E. Marsden, A mathematical introduction to fluid mechanics 1990, 1993 Springer-Verlag, New York Inc